CHALMERS | UNIVERSITY OF GOTHENBURG

PREPRINT 2008:23

A projection approach to finite volume discretization of diffusion operators

PETER HANSBO

Department of Mathematical Sciences
Division of Mathematics
CHALMERS UNIVERSITY OF TECHNOLOGY
UNIVERSITY OF GOTHENBURG
Göteborg Sweden 2008

Preprint 2008:23

A projection approach to finite volume discretization of diffusion operators

Peter Hansbo

Department of Mathematical Sciences
Division of Mathematics
Chalmers University of Technology and University of Gothenburg
SE-412 96 Göteborg, Sweden
Göteborg, May 2008

Preprint 2008:23
ISSN 1652-9715

Matematiska vetenskaper
Göteborg 2008

A projection approach to finite volume discretization of diffusion operators

Peter Hansbo
Department of Mathematical Sciences,
Chalmers University of Technology and University of Gothenburg

May 27, 2008

Abstract

We propose a new approach to cell centered finite volume discretization of elliptic problems, using triangular meshes in $\mathbb{R}^2$ as an example. In order to define derivatives of piecewise constant approximations, we first perform an L_2–projection onto the nonconforming Crouzeix–Raviart space of piecewise linear functions, and then define our discrete using a finite element approach. The resulting method has no strict limitations regarding the acuteness of angles in the mesh.

1 Introduction

The finite volume method is used extensively for fluid flow problems because it can handle unstructured meshes and has a very natural way of defining upwind differencing necessary for stability in the case of strong convection. A low order finite volume method can also be monotone (without recourse to nonlinear diffusion operators necessary in the case of finite elements), which may be desirable in some instances. However, the finite volume handling of diffusion, which is extremely simple in the case of structured grids, is a problem on unstructured grids. If the same mesh is to be used both for discretization of convection and diffusion, some (rather strong) condition on the geometry of the cells typically must be imposed, e.g., that all angles must be smaller than $\pi/2$, cf. [4]. An alternative is to mix finite element and finite volume technology and use two meshes as in the box method [2], or to use two meshes in some other, more elaborate way, see, e.g. [5].

In this note we propose another way of using finite element ideas in order to construct diffusion operators for piecewise constant approximations on triangles (or tetrahedra). The idea is to use projections of the constants onto a finite element space defined on the same mesh, followed by using the standard finite element weak form of the differential operator. This idea can then be combined with standard finite volume approximations of convective terms. We provide numerical experiments to show the properties of the resulting scheme.

2 Problem statement and finite volume discretization

We first consider the model problem of finding u such that

$$\begin{aligned} -\nabla\cdot(k\nabla u) &= f \text{ in } \Omega, \\ u &= u_D \text{ on } \partial\Omega_D, \\ k\boldsymbol{n}\cdot\nabla u &= g \text{ on } \partial\Omega_N, \end{aligned} \tag{1}$$

where Ω is a domain in $\mathbb{R}^2$ with boundary $\partial\Omega = \partial\Omega_D \cup \partial\Omega_N$, $\partial\Omega_D \cap \partial\Omega_N = \emptyset$, ∇ is the gradient operator, and k, f, g, and u_D are given functions.

We discretize Ω using a triangulation $\mathcal{T}$ consisting of triangles T and define a finite volume (FV) space by

$$W^h := \{v \in L_2(\Omega) : v|_T \in P^0(T),\ \forall T \in \mathcal{T}\}.$$

The FV approximation may be written using the basis $\{\psi_T\}$, where ψ_T is the characteristic function on T, as

$$u_0 = \sum_{T\in\mathcal{T}} U_T \psi_T(\boldsymbol{x})$$

so that each constant U_T can be interpreted as an approximation of the mean value of u on T.

A standard finite volume method can then be constructed by multiplying (1) by a test function taking the value 1 on T and zero elsewhere, and use integration by parts so that

$$\int_T f\,dx = -\int_{\partial T} k\,\boldsymbol{n}_T \cdot \nabla u\,ds,$$

where $\boldsymbol{n}_T$ is the outward pointing normal on T, and the problem is to find a way of using u_0 to approximate $\boldsymbol{n}_T \cdot \nabla u$ across element borders using a sufficiently accurate difference stencil in such a way that neighbouring elements agree on what the normal derivative is. These requirements are easy to fulfill on a structured grid, but turn out to be rather difficult to satisfy on arbitrary grids.

In this paper, we shall instead introduce an intermediate finite element (FE) space V^h and define our discrete approximation as

$$u_h := P_h u_0 = \sum_i U_i P_h \psi_i, \tag{2}$$

where P_h denotes the L_2–projection onto V_h, defined by seeking $P_h u \in V^h$ such that

$$\int_\Omega P_h u\, v_h\,d\Omega = \int_\Omega u\, v_h\,d\Omega, \quad \forall v_h \in V^h. \tag{3}$$

It is desirable to select V^h in such a way that the number of interconnections are as small as possible. For example, if V^h is the space of piecewise linear, continuous functions, then the mass matrix is not diagonal and has to be inverted. It can be lumped, which alleviates this problem, but in any case $P_h\psi_T$ will be nonzero on all elements sharing a vertex with T. This number changes from element to element in an unstructured mesh, making an efficient implementation more difficult. For this reason, we choose to use a non-conforming FE space V^h, more precisely the Crouzeix-Raviart space [3]

$$V^h := \{v : v|_T \in P^1(T) : \int_e [v]\,ds = 0,\ \forall e \in \mathcal{E}_I\},$$

where $\mathcal{E}_I$ denotes the set of all internal element edges in the mesh and $[v]$ denotes the jump across the edge. We further split the boundary edges into two sets; edges on $\partial\Omega_D$ make up the set $\mathcal{E}_D$, and those on $\partial\Omega_N$ make up the set $\mathcal{E}_N$.

Since the approximation is linear, this space can be easily constructed using nodes on the midpoints of the edges in the mesh (faces in $\mathbb{R}^3$). Continuity in these nodes then guarantees that the mean value of discrete functions are zero along internal edges. For this space, the mass matrix is diagonal and $P_h\psi_T$ is nonzero only on T and its neighbors. A typical patch consisting of T and its neighbors together with the constant basis function and its projection is shown in Figure 1.

We remark that the only difference on tetrahedra in $\mathbb{R}^3$ is that the diagonality of the mass matrix is lost. This can however be reintroduced by mass lumping, and thus the method extends to this case.

Introducing the notation

$$(f,v)_h := \sum_{T\in\mathcal{T}} \int_T f\,v\,dxdy, \quad a_h(u,v) := \sum_{T\in\mathcal{T}} \int_T \nabla u \cdot \nabla v\,dxdy,$$

we now propose the following method: find $u_0 \in W^h$ such that

$$\begin{aligned} a_h(P_h u_0, P_h v_0)_h + \sum_{e\in\mathcal{E}_D} \int_e \frac{\gamma\, k}{h} P_h u_0 P_h v_0 \, ds = (f, P_h v_0)_h \\ + \sum_{e\in\mathcal{E}_D} \int_e \frac{\gamma\, k}{h} u_D P_h v_0 \, ds + \sum_{e\in\mathcal{E}_N} \int_e g P_h v_0 \, ds \quad \forall v_0 \in W^h, \end{aligned} \tag{4}$$

where h denotes the local element size and γ a dimensionless penalty parameter. Wee choose this penalty formulation, first suggested by Babuška [1], because of the intrinsic difficulty of prescribing $P_h u_0$ strongly on $\partial\Omega_D$ (an alternative, also used in the numerical examples, is to set the values on the triangles bordering to the Dirichlet boundary strongly).

Regarding the practical implementation, one can use the standard FE technique of integrating the bilinear form $a_h(\cdot,\cdot)$ element by element. In doing so, one has to take into account all those shape functions that interact on the element in question. The shape function of this element interacts with itself and those of the element's neighbours, and, unlike a standard finite element method, the shape function of each neighbour also interacts with the shape functions of the remaining neighbours. Apart from this last (minor) point, standard FE technology can be used.

3 Convection–diffusion

We finally consider the extension to convection–diffusion problems of the type

$$\begin{aligned} \nabla\cdot(\boldsymbol{c}\, u - k\nabla u) &= f \text{ in } \Omega, \\ u &= u_D \text{ on } \partial\Omega_D, \\ k\boldsymbol{n}\cdot\nabla u &= g \text{ on } \partial\Omega_N, \end{aligned} \tag{5}$$

where $\boldsymbol{c}$ is a given convective velocity field. The simplest way of obtaining a stable discretization of the convective term is to use the standard finite volume upwind method. To this end, we identify all sides of elements on the upwind side: on a given element T we define

$$\partial T_{\text{upw}} := \{\partial T :\ \boldsymbol{n}_T \cdot \boldsymbol{c} < 0\},$$

and seek $u_0 \in W^h$ such that

$$\begin{aligned} a_h(P_h u_0, P_h v_0)_h + \sum_{e\in\mathcal{E}_D} \int_e \frac{\gamma\, k}{h} P_h u_0 P_h v_0 \, ds + \sum_{T\in\mathcal{T}} \int_{\partial T_{\text{upw}}} |\boldsymbol{c}\cdot\boldsymbol{n}_T|\,[u_0]\, v_0 \, ds \\ = (f, P_h v_0)_h + \sum_{e\in\mathcal{E}_D} \int_e \frac{\gamma\, k}{h} u_D P_h v_0 \, ds + \sum_{e\in\mathcal{E}_N} \int_e g P_h v_0 \, ds \quad \forall v_0 \in W^h, \end{aligned} \tag{6}$$

where $[u_0]$ denotes the jump $\lim_{\epsilon\downarrow 0} u_0(\boldsymbol{x} + \epsilon\boldsymbol{n}_T) - u_0(\boldsymbol{x} - \epsilon\boldsymbol{n}_T)$ and we set $u_0(\boldsymbol{x} + \epsilon\boldsymbol{n}_T) := u_D$ in case $\partial T_{\text{upw}} \cap \partial\Omega_D \neq \emptyset$.

4 Numerical examples

4.1 Convergence

The first numerical example concerns the convergence of the method using different balances between diffusion and convection. We consider the domain $\Omega = (0,1)\times(0,1)$ and the exact solution $u = x\,(1-x)\,y\,(1-y)$. Inserting this solution into the convection–diffusion equation (5), we find that the corresponding right–hand side is

$$f = c_x(2x-1)(y-1)y + c_y(x-1)(2y-1)x - 2k(x(x-1)+y(y-1)).$$

Here the boundary conditions were imposed strongly by setting $u_0 = 0$ on those element having a side on the boundary. We run three test: first with $\boldsymbol{c} = 0$ and $k = 1$, then with $\boldsymbol{c} = (2,1)$ and

$k = 1$, and finally $\boldsymbol{c} = (2, 1)$ and $k = 10^{-6}$. We observe that for a pure diffusion case, we have second order convergence of the projected solution, first order convergence in a broken H^1-norm of the projected solution, and first order convergence of the non–projected solution, see Figure 5. The second order convergence can probably not be guaranteed on all sequences of refined meshes since we do not have a fully linear FE space to work with. It is likely that some sort of local symmetry is necessary. The second order convergence of the L_2–norm is anyway lost when convection is introduced, while the first order convergence of the broken H^1–norm remains until the problem is convection dominated, in which case only convergence in L_2 remains, see Figures 3–4. Finally, in Figures 5–6 we show elevations of the projected solution in the pure diffusion and the convection dominated cases, shown on the same mesh. Note the oscillating character of the projected solution in the second case, which precludes H^1–convergence.

4.2 Stability

The diffusion discretization works on more general meshes than standard finite volume discretizations of diffusion, but it fails as the largest angle $\alpha \to \pi$. In order to illustrate the sensitivity to the largest angle, we solve a problem on a variable rectangular domain $\Omega = (0, x_{\max}) \times (0, 1)$ with exact solution

$$u = \frac{x\,(x_{\max} - x)\,y\,(1 - y)}{x_{\max}^2},$$

using a fixed triangulation. By increasing $x_{\max}$, we obtain triangles with increasing α. In FIgure 7 we show a log-log plot of the L_2–error of the projected solution as a function of α/π. Though the meshsize changes, and thus affects the L_2–error, this plot nevertheless shows a loss of stability in the solution as $\alpha \to \pi$. The stretch for the last datapoint corresponds to $x_{\max} = 256$, and we conclude that the method is capable of handling large angles as long as they are not too close to π.

4.3 Resolution of layers

The final problem is a boundary layer problem where the boundary conditions are $u = 0$ at $x = 1$and $y = 0$, $u = 1$ at $x = 0$ and $y = 1$. Here we used weak boundary conditions. The convective velocity was set to $\boldsymbol{c} = (2, 1)$, and in Figures 8–9 we show the numerical results obtained with $k = 0.1$, $k = 0.01$, $k = 0.001$, and $k = 0.0001$. The origin is in the upper left corner and the perspective is from $x > 1$.

5 Concluding remarks

We have introduced a way of discretizing diffusion operators for finite volume methods that work also on distorted meshes and which does not require dual meshes. Numerical examples suggest first order convergence in L_2 for a wide range of diffusion to convection ratio, using a first order upwind scheme for the convection part.

References

[1] Babuška I. The finite element method with penalty. *Mathematics of Computation* 1973; **27**(122):221–228.

[2] Bank RE, Rose DJ. Some error estimates for the box method, *SIAM Journal of Numerical Analysis* 1987; **24**(4):777–787.

[3] Crouzeix M, Raviart PA. Conforming and nonconforming finite element methods for solving the stationary Stokes equations, *RAIRO Analyse Numerique* 1973; **7**:33–75.

[4] Herbin R. An error estimate for a finite volume scheme for a diffusion–convection problem on a triangular mesh, *Numerical Methods for Partial Differential Equations* 1995; **11**(2):165–173.

[5] Hermeline F. A finite volume method for the approximation of diffusion operators on distorted meshes, *Journal of Computational Physics* 2000; **160**(2):481–499.

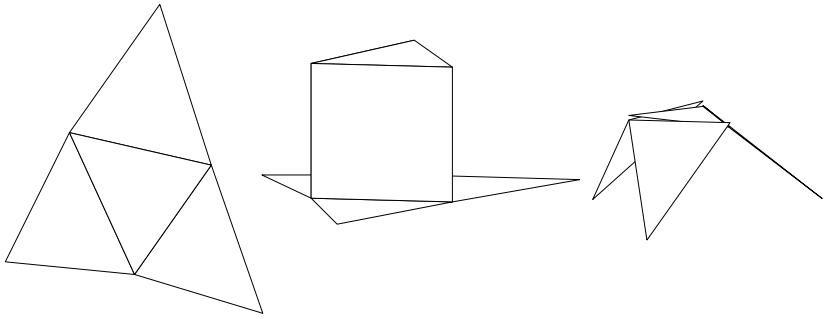

Figure 1: A patch surrounding T, with ψ_T and $P_h\psi_T$.

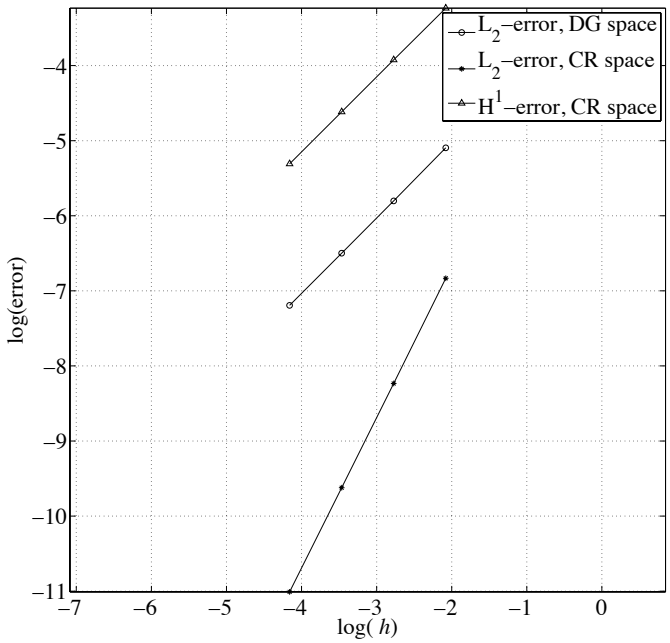

Figure 2: Convergence in the pure diffusion case.

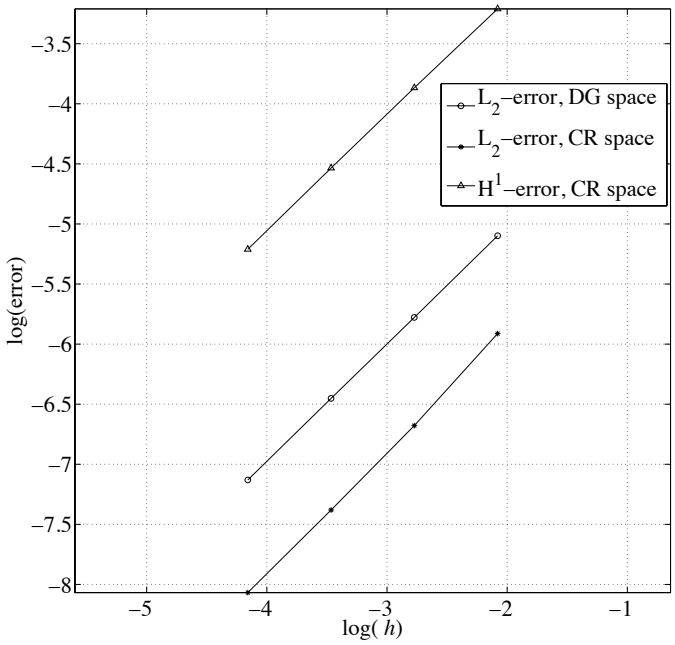

Figure 3: Convergence in the diffusion dominated case.

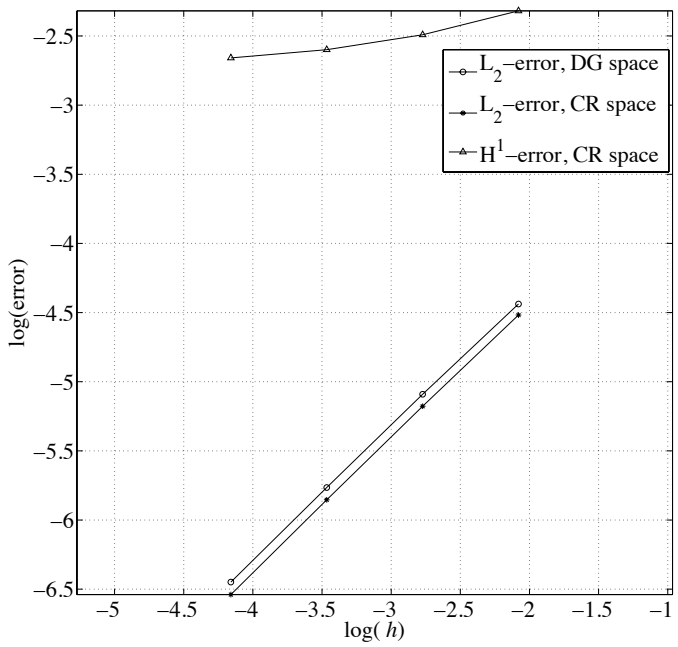

Figure 4: Convergence in the convection dominated case.

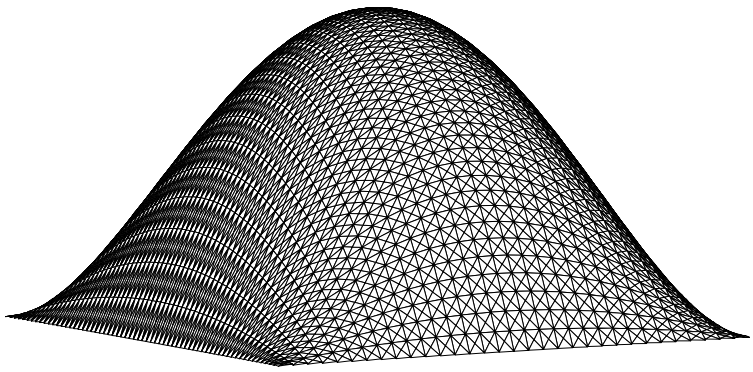

Figure 5: Elevation of the (projected) pure diffusion solution.

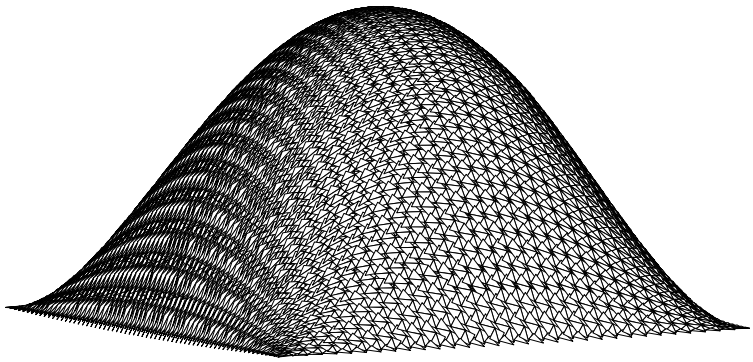

Figure 6: Elevation of the (projected) solution in the convection dominated case.

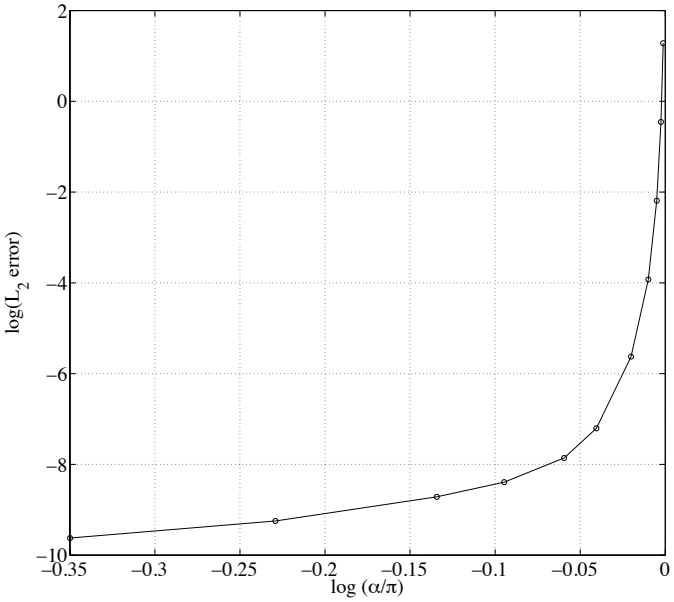

Figure 7: L_2 error as a function of largest angle.

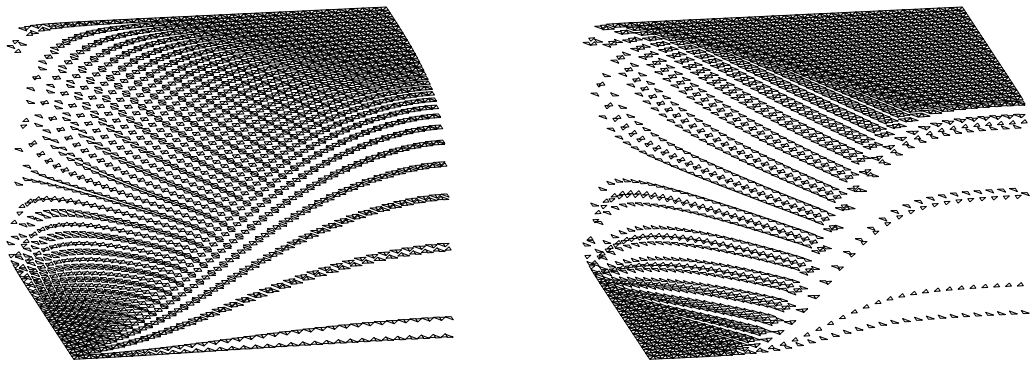

Figure 8: Elevation of the solution for $k = 1/10$ and $k = 1/100$.

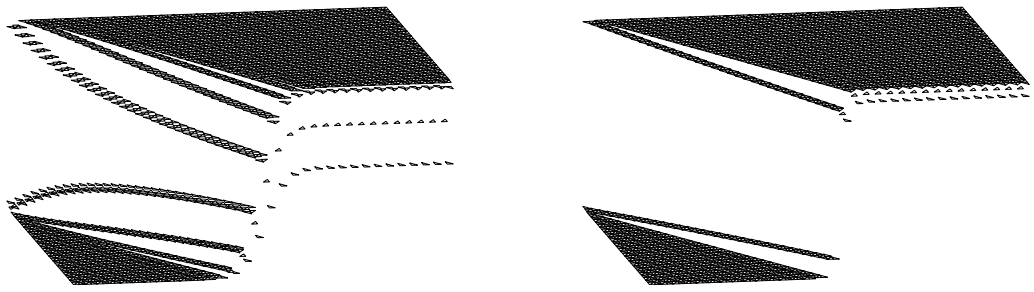

Figure 9: Elevation of the solution for $k = 10^{-3}$ and $k = 10^{-4}$.